Available online at www.sciencedirect.com

ScienceDirect

Geochimica et Cosmochimica Acta 233 (2018) 66–80

Geochimica et Cosmochimica Acta

www.elsevier.com/locate/gca

Cadmium cycling in the water column of the Kuroshio-Oyashio Extension region: Insights from dissolved and particulate isotopic composition

Shun-Chung Yang [a], Jing Zhang [b], Yoshiki Sohrin [c], Tung-Yuan Ho [a,d,*]

[a] *Research Center for Environmental Changes, Academia Sinica, Taipei, Taiwan*
[b] *Department of Environmental Biology and Chemistry, University of Toyama, Toyama, Japan*
[c] *Institute for Chemical Research, Kyoto University, Kyoto, Japan*
[d] *Institute of Oceanography, National Taiwan University, Taipei, Taiwan*

Received 30 August 2017; accepted in revised form 1 May 2018; Available online 9 May 2018

Abstract

We measured dissolved and particulate Cd isotopic composition in the water column of a meridional transect across the Kuroshio-Oyashio Extension region in a Japanese GEOTRACES cruise to investigate the relative influence of physical and biogeochemical processes on Cd cycling in the Northwestern Pacific Ocean. Located at 30–50°N along 165°E, the transect across the extension region possesses dramatic hydrographic contrast. Cold surface water and a relatively narrow and shallow thermocline characterizes the Oyashio Extension region in contrast to a relatively warm and highly stratified surface water and thermocline in the Kuroshio Extension region. The contrasting hydrographic distinction at the study site provides us with an ideal platform to investigate the spatial variations of Cd isotope fractionation systems in the ocean. Particulate samples demonstrated biologically preferential uptake of light Cd isotopes, and the fractionation effect varied dramatically in the surface water of the two regions, with relatively large fractionation factors in the Oyashio region. Based on the relationship of dissolved Cd concentrations and isotopic composition, we found that a closed system fractionation model can reasonably explain the relationship in the Kuroshio region. However, using dissolved Cd isotopic data, either a closed system or steady-state open system fractionation model may explain the relationship in the surface water of the Oyashio region. Particulate $\delta^{114/110}$Cd data further supports that the surface water of the Oyashio region matches a steady-state open system model more closely. Contrary to the surface water, the distribution of potential density exhibits comparable patterns with Cd elemental and isotopic composition in the thermocline and deep water in the two extension regions, showing that physical processes are the dominant forcing controlling Cd cycling in the deep waters. The results demonstrate that Cd isotope fractionation can match either a closed or open system Rayleigh fractionation model, depending on the relative contribution of physical and biogeochemical processes on its cycling.

Keywords: GEOTRACES; Cadmium; Dissolved; Particulate; Isotopic composition; Biogeochemical cycling; Biogeochemical and physical processes; Kuroshio-Oyashio extension

1. INTRODUCTION

Cadmium has captured the attention of oceanographers and marine geochemists since 1970s due to its unique features in the ocean, particularly for its nutrient type distribution

* Corresponding author at: Research Center for Environmental Changes, Academia Sinica, 128, Sec. 2, Academia Rd., Nankang, Taipei 115, Taiwan.
E-mail address: tyho@gate.sinica.edu.tw (T.-Y. Ho).

https://doi.org/10.1016/j.gca.2018.05.001
0016-7037/

and close interaction with phytoplankton (Boyle et al., 1976; Price and Morel, 1990; Sunda and Huntsman, 2000). Similar to major nutrients, depleted Cd concentrations in oceanic surface water are attributed to efficient uptake by phytoplankton and relatively low external input. Subsurface water advection and diffusion have been recognized as the major Cd source in surface water (Martin and Thomas, 1994). However, with comparable vertical distribution patterns across the major oceans, Cd concentrations alone provide limited information on the controlling processes for its vertical cycling in the ocean. Measurement of Cd isotopic composition may provide further information on understanding the processes at work in oceanic systems (Ripperger et al., 2007).

Indeed, studies of Cd isotopic composition in seawater have revealed new insights into the major processes influencing Cd cycling in oceans since 2006. The early studies observed distinct vertical Cd isotopic variations globally, with relatively consistent values in deep waters and relatively heavy and diverse values in oceanic surface waters (Lacan et al., 2006; Ripperger et al., 2007). It has been proposed that phytoplankton preferentially take up light Cd isotopes in the euphotic zone and results in relatively heavy Cd isotopic compositions in the surface water (Lacan et al., 2006; Ripperger et al., 2007). This argument was further supported by later laboratory and field studies (John and Conway, 2014; Yang et al., 2015). In comparison to surface water, dissolved $\delta^{114/110}$Cd variations in thermocline and deep waters are relatively small, generally less than 0.5‰ ($\delta^{114/110}Cd = [(^{114}Cd/^{110}Cd)_{sample}/(^{114}Cd/^{110}Cd)_{NIST\ 3108} - 1] \times 10^3$) (Abouchami et al., 2014; Conway and John, 2015; John et al., 2017; Janssen et al., 2017). Recent large scale studies observed that the Cd isotopic variations in the deep water are closely correlated with the changes of water temperature and salinity, indicating that physical forcings, mainly through water advection and mixing, are the dominant processes controlling Cd isotopic composition in thermocline and deep waters horizontally (Abouchami et al., 2014; Conway and John, 2015; John et al., 2017; Xie et al., 2017).

While there is consensus that physical processes are the major factors regulating Cd isotopic composition in oceanic deep water (e.g. Conway and John, 2015; Janssen et al., 2017; Xie et al., 2017), proposed controlling mechanisms for Cd isotope fractionation patterns in oceanic surface water and across the thermocline seem to be spatially and temporally variable. Several studies observed the preferential removal of light Cd isotopes through Cd scavenging processes in oxygen deficient zones and argued that these precipitation process may be an important sink for dissolved Cd in the ocean (Janssen et al., 2014; Conway and John, 2015). Supported by the Cd isotopic composition in suspended and sinking particles collected in the surface water, our previous study argued that the fractionation effect of microbial degradation opposed that of phytoplankton uptake and resulted in insignificant net biological fractionation effects in the surface water of the South China Sea (Yang et al., 2012; 2015). In addition to a typical simple closed system Rayleigh fractionation model (Ripperger et al., 2007; Abouchami et al., 2011, 2014), a steady-state open system fractionation model has also been proposed to describe the fractionation behaviors of Cd isotopes in oceanic surface waters (Xue et al., 2013; Xie et al., 2017).

If Cd isotopic cycling is mainly regulated by phytoplankton fractionation coupled with the export of sinking particles in surface water and limited external Cd input in the surface water, the fractionation pattern should follow a typical closed Rayleigh fractionation system in the surface water. In a closed system, since phytoplankton preferentially takes up light Cd isotopes and the plankton organic material is exported out of the surface water through particle sinking, dissolved $\delta^{114/110}$Cd in the surface water would thus linearly increase with decreasing Cd concentrations in log scale expression (Ripperger et al., 2007). This kind of fractionation phenomenon has been demonstrated in the Atlantic sector of the Southern Ocean, where Cd concentrations progressively decreased with increasing $\delta^{114/110}$Cd in the surface water generating a well-defined linear relationship between $\delta^{114/110}$Cd and Cd concentrations on a log scale (Abouchami et al., 2011, 2014). However, several studies showed that the closed system model cannot explain the elemental and isotopic relationship in the surface waters of other oceanic regions, such as Southwest Atlantic and the Pacific sector of the Southern Ocean (Gault-Ringold et al., 2012; Xie et al., 2017). The studies show that for sample concentrations less than 0.1 nM in these oceanic regions, Cd isotopic composition does not exhibit a log-linear relationship with Cd concentrations in log scale. Instead it reached a constant value within the low concentration range. To explain the fractionation pattern, Xie et al. (2017) suggested that the surface water for Cd cycling was a steady-state open system. They proposed that the removal of Cd through particle sinking was balanced by the supply of Cd through diapycnal mixing. In an open system, it is proposed that the vertical supply of relatively light Cd from subsurface water balances the export of relatively light Cd through particle sinking in the surface water and results in a constant $\delta^{114/110}$Cd value with decreasing Cd concentrations in the surface water (Xie et al., 2017). Moreover, a study in the subarctic northeast Pacific observed that the Cd isotope fractionation pattern followed a simple closed system model in 2012 but the pattern converted to the open system model in 2014. This was most likely due to the influence of the formation of other water masses regionally in the surface water (Janssen et al., 2017). Further effort is still required to fully understand how Cd isotope fractionation patterns in oceanic surface water are regulated by various environmental factors globally.

With contrasting hydrographic settings along the Kuroshio-Oyashio Extension transect, this region provides an ideal platform to evaluate the relative importance of major physical and biogeochemical processes controlling Cd isotope fractionation systems. This extension region is comprised of a northern section and a southern section, which are represented by the extremely cold and relatively productive water mass in the Oyashio Extension region (hereafter the Oyashio region) and the warm and relatively stratified oligotrophic water mass in the Kuroshio Extension region (hereafter the Kuroshio region) (Figs. 1 and 2). In this study, we analyzed the dissolved and particulate Cd isotopic composition and Cd concentrations,

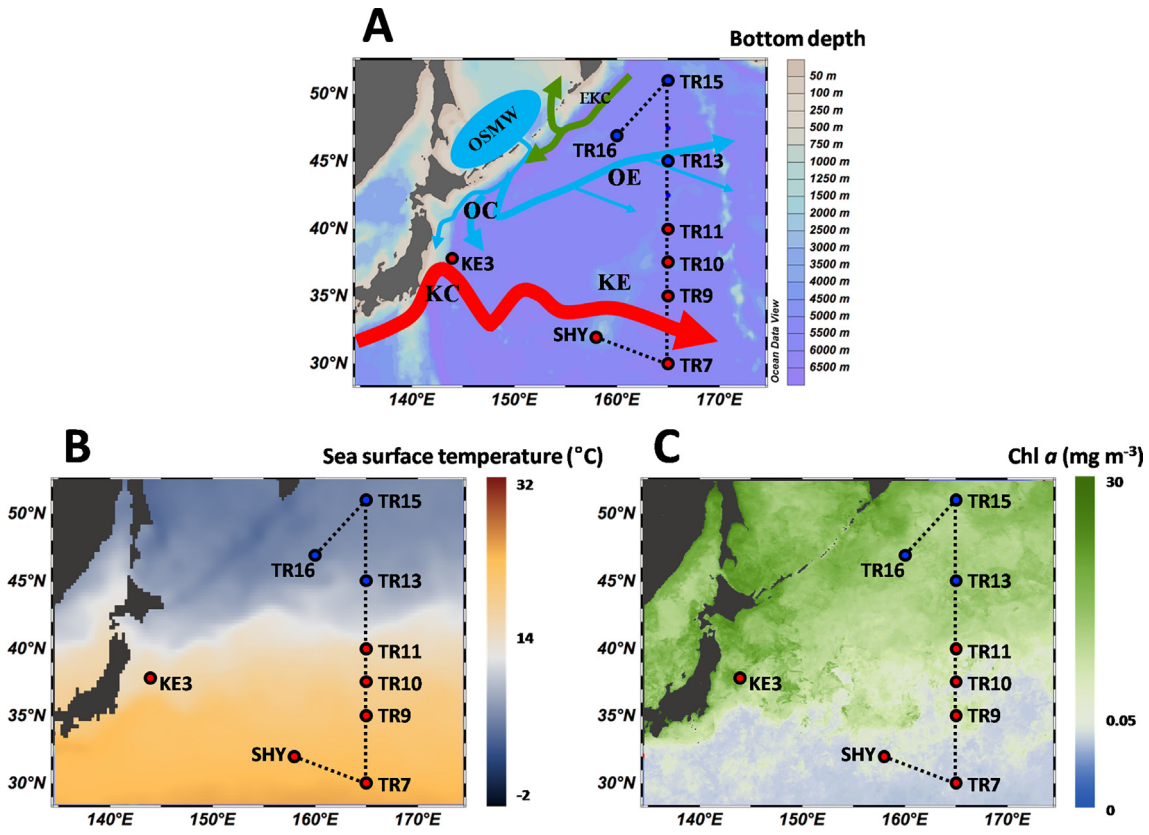

Fig. 1. Locations of sampling stations and the sea surface temperature and averaged chlorophyll *a* concentrations in 2011. The major surface currents and bottom depths (A), sea surface temperature (B), and chlorophyll *a* concentration (C). KC: Kuroshio Current, OC: Oyashio Current, KE: Kuroshio Extension, OE: Oyashio Extension, OSMW: Okhotsk Sea Mode Water, EKC: East Kamchatka Current. Circles in red stand for stations in KE region; circles in blue stand for stations in OE region. Sea surface temperature and chlorophyll *a* concentrations are 2011 annual average obtained from NOAA satellite database (website: https://www.nnvl.noaa.gov).

as well as other related environmental parameters in the water column of both regions to investigate how physical and biogeochemical processes influence Cd isotope fractionation patterns in the oceanic surface waters of the Oyashio and Kuroshio regions.

2. METHOD

2.1. Hydrographic background of study site

This study was carried out on a Japanese GEOTRACES cruise KH-11-07, also known as GEOTRACES cruise section GP18, by R/V Hakuho-Maru in July 2011. The study area crossing over the Kuroshio-Oyashio Extension region, is located at a latitudinal section from 30° to 50°N along 165°E and includes six sampling stations along 165°E and two sampling stations at 32.0°N, 157.9°E and 47.0°N, 160.1°E (Fig. 1A, Table S1). In the top 200 m of the Oyashio Extension region from 50° to 40°N, the water is composed of water masses with salinity values ranging from 32.7 to 33.8 and temperatures ranging from 0.9 to 11.1 °C (Fig. 2A and B). The waters are transported to the region by the Oyashio current from the subarctic area, where precipitation exceeds evaporation (Yasuda, 2004). Below the surface water layer is Okhotsk Sea Mode Water (OSMW), characterized by potential density (σ_θ) values ranging from 26.6 to 27.0 at the depths of 200–400 m (Fig. 2A) (You et al., 2000). This mode water originates in the Sea of Okhotsk, flows out to the Pacific through the Kuril Straits, and then travels to the extension region through the Oyashio current as well (You et al., 2000).

In the Kuroshio Extension region, from 30° to 40°N, the surface water is composed of water masses with salinity values of over 34.3 and temperatures over 10 °C in the top 200 m (Fig. 2A and B). The surface waters originate from the tropical Pacific and are transported to the extension region through the Kuroshio current (Yasuda, 2003). Beneath the surface waters are Subtropical Mode Water (STMW) and Central Mode Water (CMW), with σ_θ values ranging from 25.2 to 25.8 and 26.0 to 26.7, respectively (Fig. 2A) (Yasuda, 2003). The formation region of STMW is located at 32–35°N and 140–180°E in the subtropical northwest Pacific, and the formation region of CMW generally covers the area of 36–43°N within the range of 150°E to 160°W of the central north Pacific Ocean (Yasuda, 2003). Underlying STMW and CMW is North Pacific Intermediate Water (NPIW), a widely distributed water mass in the North Pacific subtropical gyre characterized with a salinity minimum

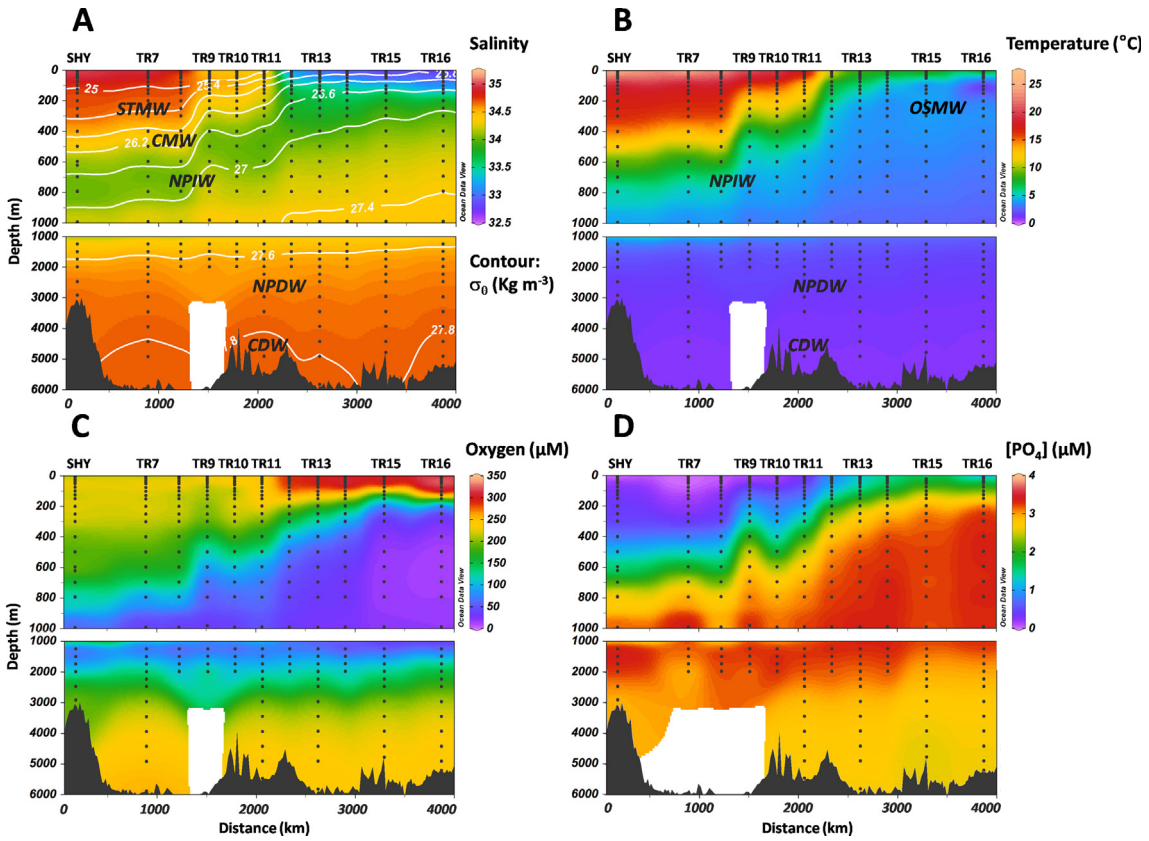

Fig. 2. Transects of potential density (σ_θ) and salinity (A), potential temperature (B), dissolved oxygen (C) and phosphate (D) of the studied region.

centered at $\sigma_\theta = 26.8$ (Fig. 2A) (Yasuda, 2004). The low-salinity signature in this water mass mainly comes from the subarctic area, as a large part of the low-salinity Oyashio water flows southward. It sinks to intermediate depths in the subtropical gyre to form NPIW (Yasuda, 2004).

North Pacific Deep Water (NPDW) is distributed in the zonation deeper than 2500 m, characterized by temperatures between 1.2 and 2 °C and high levels of major nutrients and low oxygen concentrations (Fig. 2B–D), where phosphate concentrations are up to 3 μM and dissolved oxygen concentrations are down to 60 μM (Fiedler and Talley, 2006). Bottom water deeper than 4000 m is mainly composed of Circumpolar Deep Water (CDW), characterized by relatively high oxygen and low nutrient concentrations compared with NPDW (Fig. 2C and D) (Fiedler and Talley, 2006). The CDW originates from water mixing between Antarctic Bottom Water and North Atlantic Deep Water (Fiedler and Talley, 2006).

2.2. Sampling and pretreatment

Seawater and suspended particle samples were collected with pre-cleaned Teflon-coated Niskin-X samplers (General Oceanics) from July 19 to July 30 in 2011. The sampling bottles were cleaned using 1% alkaline surfactant (Extran MA01), 0.1 M HCl (Special Grade, Wako Pure Chemical Industries) and Millipore Milli-Q water (18.2 MΩ cm^{-1}). Samplers were equipped on a polyurethane coating Al hydrocast and deployed by using Kevlar wire. For subsampling, the Niskin-X samplers were detached from the hydrocast, and carefully moved into a clean space (filled with air which was passed through a HEPA filter) in the onboard laboratory of the research vessel. Seawater was filtered through inline 0.22 μm acid-cleaned POLYCAP cartridge filters (Whatman® Nuclepore™), and subsequently transferred to acid-washed 500 mL polyethylene bottles (Nalgene) after rinsing more than three times using filtered seawater and acidified to pH 1 with ultrapure HCl (Seastar) immediately following collection. Blank samples were obtained on board by pouring 500 mL Milli-Q water into polyethylene bottles and the water was also acidified with ultrapure HCl as samples treated. After filtered seawater sampling, unfiltered seawater was collected via acid-cleaned silicon tubing into acid-washed 500 mL polyethylene bottles after rinsing more than three times using the same water. Suspended particle samples were collected in the onboard clean room (Room 4) by filtering 500 mL unfiltered seawater collected from the top 400 m water depths through an acid-washed polypropylene filter holder with 47 mm 0.2 μm acid-washed polycarbonate membranes. The holder was connected with a pump with vacuum pressure kept under 15 kPa during the filtration. Filters with particle samples were then sealed in acid-washed Teflon vials and stored under −20 °C before pretreatment. Particle

blanks were obtained by passing 500 mL filtered surface seawater through clean filters.

For filter sample digestion, each filter membrane with suspended particle samples was attached to the vial wall of a 15 mL acid-washed Teflon vial containing a 5 mL 8 M super pure HNO_3 (Seastar) and 2.9 M super pure HF (Seastar) mixture. Then, the filter samples were digested on a hot plate at 120 °C for 12 h (Cullen and Sherrell, 1999). After digestion, the membranes were taken out by acid-washed Teflon forceps and rinsed with 2 mL Milli-Q water right above the digestion vials to collect the rinsing solution into the same vials. The digested solution was then heated on a hot plate at 80 °C in a trace-metal clean hood to nearly dry. Digested and dried particle samples were re-dissolved by adding 5 mL 0.5 M super pure HNO_3 then approximately 0.5 mL of the sample solution was taken for elemental and Cd isotopic analysis.

Dissolved Cd concentrations were determined by three different methods, including two methods applying chelating resin pretreatment with HR-ICPMS analysis (Sohrin et al., 2008; Ho et al., 2010) and one applying double spike with MC-ICPMS analysis (Yang et al., 2012). Seawater samples were filtered and analyzed independently by the two research groups of Yoshiki Sohrin and Tung-Yuan Ho. Dissolved Cd concentrations in 120 or 40 mL filtered samples were either semi-automatically or fully automatically preconcentrated by chelating resins pretreatment systems by the methods of Sohrin et al. (2008) and Ho et al. (2010), respectively. The preconcentrated samples were then analyzed by HR-ICPMS. Cd concentrations were also determined by the double spike technique in this study. The accuracy of the Cd concentrations was validated by analysis of a reference material (NASS-6) and intercalibration of the two laboratories. The inter-laboratory comparison indicates that majority of the measurements were statistically comparable (Fig. S1 and Table S2).

We used a double spike technique to obtain precise Cd content and isotopic composition in seawater and particle samples. Approximately 500 mL of seawater at each sampling depth was taken for Cd isotopic composition analysis. Seawater samples were first combined with a suitable mass of Cd double spike (^{110}Cd–^{111}Cd) to achieve a sample to spike ratio of 1:4. Spiked samples were then left in clean room for at least 3 days to reach full sample-spike equilibration. Before carrying out chemical separation procedures, $CH_3CHOONH_3$ and NH_4OH were added to seawater samples to adjust pH to approximately 6. A three-stage ion exchange chemical separation procedure adapted from the studies of Ripperger and Rehkämper (2007) and Conway et al. (2013) was used for Cd purification. Nobias PA-1 resin was used to preconcentrate Cd in seawater samples and remove major elements. Anion resin AG1X8 (Biorad) was then used to remove specific elements that cause interferences in Cd isotopic analysis, such as Sn and Zn. Finally, the anion resin, TRU (Eichrom), was used to further remove Mo and Sn to avoid their isobaric interferences during Cd isotopic analysis. The Cd double spike was added to digested particle samples to achieve a sample to spike ratio of 1:4 as well. The samples were evaporated to dryness on a hot plate held at 80 °C in a trace-metal clean hood, re-dissolved in 0.1 mL super pure HCl (Seastar), evaporated to dryness, and then dissolved in 1.4 mL 0.7 M super pure HCl. The samples were then separated using a three-stage ion exchange procedure as described in the study of Yang et al. (2015). Resin AG1X8 was used in the first and the second stages, and resin TRU resin was used in the third stage to purify Cd from the samples.

The chemically purified Cd samples were evaporated to dryness and refluxed in 1 mL of 16 M HNO_3 and 0.1 mL of 35% H_2O_2 at 160 °C for at least 6 h to decompose any left-over organic matter (Gault-Ringold and Stirling, 2012; Takano et al., 2017). Then samples were evaporated to dryness again and were re-dissolved with 0.5 M of super pure nitric acid to achieve a final sample concentration of approximately 5–10 ng g^{-1}Cd. The seawater and particle blank samples were treated with the same pretreatment procedures as the samples. Overall, the background Cd in the blank seawater ranged from 2 to 14 pg (5 ± 5 pg on average, 1 σ and $n = 5$) for sampling and Cd purification, which is equivalent to 0.037–0.25 pM (0.10 ± 0.09 pM) of dissolved Cd in seawater. This blank accounts for around 0.01% of deep water samples and 3% of surface water samples. Overall, the detection limit of this method for dissolved Cd concentration is around 0.27 pM. The particle blank mass ranged from 4 to 16 pg (8 ± 3 pg on average, 1 σ and $n = 10$) for sampling and purification procedures, which is equivalent to 0.079–0.28 pM (0.14 ± 0.06 pM) of particulate Cd in seawater, accounting for 1–4% of Cd mass in sample filters. The reported concentrations are all blank corrected. The Cd mass in the blanks were too low to obtain meaningful isotopic composition information so that the isotopic composition measurements were not blank corrected, as is usual during Cd isotopic analysis as the blank contribution is insignificant. Other detailed pretreatment information may be found in our previous studies (Yang et al., 2012; 2015).

2.3. MC-ICPMS analysis

The details for Cd isotopic analysis are also described in our previous studies (Yang et al., 2012, 2015). Briefly, all of the Cd isotopic measurements were performed using a multi-collector ICP-MS (Thermo Neptune) with a desolvator nebulizer as the sample introduction system (ESI Apex-IR). Four Cd isotopes, ^{110}Cd, ^{111}Cd, ^{112}Cd, and ^{114}Cd, were simultaneously measured in each analysis. Potential isobaric interferences from ^{110}Pd, ^{112}Sn and ^{114}Sn were corrected within-run by simultaneously monitoring ^{105}Pd and ^{117}Sn. The instrumental settings are shown in Table S3. All of the Cd isotopic compositions in this study are reported in δ-notation, which is given by the following equation:

$$\delta^{114/110}\mathrm{Cd} = \left[\left(^{114}\mathrm{Cd}/^{110}\mathrm{Cd}\right)_{\mathrm{sample}} / \left(^{114}\mathrm{Cd}/^{110}\mathrm{Cd}\right)_{\mathrm{standard}} - 1\right] \times 10^3$$

We have used NIST SRM 3108 as the primary reference standard for normalization purposes. The within-day external reproducibility and internal precision for standard measurement ranged from ±0.05 to ±0.11‰ (2σ, $n = 5$) and from ±0.02 to ±0.09‰ (2σ, 63 runs per measurement), respectively. The precision was obtained by repeatedly

analyzing the Cd standard JMC Cd Münster (ICP standard, lot 502552A). The analytical precision for the reported Cd isotopic composition of each sample was obtained by combining the internal precision of both sample and standard measurements (Yang et al., 2015). The accuracy of the analysis was verified by routinely determining the Cd isotopic composition of the following two international Cd standards, NIST SRM 3108 and JMC Cd Münster, on the same day. The value we obtained for JMC Cd Munster was normalized to NIST SRM 3108, which yielded the averaged isotopic composition of -0.10 ± 0.02‰ (2σ, n = 44) for JMC Cd Münster, consistent with the validated value of -0.08 ± 0.04‰ reported previously (Abouchami et al., 2012). Our in-house standard, Alfa Aesar Cd Metal (Puratronic Cd metal, lot J16 L23), was also measured during the analysis period for sample measurements and gave an average value of -1.21 ± 0.03‰ (2σ, n = 23), which is in agreement with the value we had reported previously of -1.29 ± 0.16‰ (2σ, n = 32) (Yang et al., 2012).

3. RESULTS

3.1. Spatial distribution of dissolved Cd: the Kuroshio region

The spatial distributions of dissolved Cd concentrations and $\delta^{114/110}$Cd are shown in Figs. 3 and 4 and Table S4. The distribution patterns are comparable to temperature and other major hydrographic parameters (Fig. 2; Tables S1 and S5), with relatively high Cd concentrations and low Cd isotopic compositions in the Oyashio region and a significant vertical gradient in the Kuroshio region. In the Kuroshio region, dissolved Cd in the surface water was depleted and its Cd isotopic composition was relatively heavy, with concentrations down to 3.3 pM and a Cd isotopic value up to +1.0‰ (Fig. 4). With increasing depth from the water surface to 200 m, the Cd concentration increased from 3.3 pM to 0.16 nM and the $\delta^{114/110}$Cd value ranged from +0.8 to +0.4‰ (Fig. 3). From 200 to 500 m, dissolved Cd concentrations increased from 0.16 to 0.56 nM and the $\delta^{114/110}$Cd value slightly decreased from +0.4 to +0.3‰ (Fig. 3), exhibiting similar distribution patterns in the two dominant water masses, STMW and CMW (Fig. 2A). Within the NPIW zone, located at a depth interval of 500–1000 m with a minimal salinity of 34.0 at its core (Fig. 2A), dissolved Cd concentrations gradually increased from 0.56 to 0.95 nM with depth and the $\delta^{114/110}$Cd remained at +0.3‰ (Fig. 3). Below NPIW, dissolved Cd concentrations increased to a maximum value of ~1 nM in the deep water zone. Here the salinity ranged from 34.6 to 34.3 and the σ_θ ranged from 27.7 to 27.4, while the $\delta^{114/110}$Cd remained similar to the values observed in NPIW.

3.2. Spatial distribution of dissolved Cd: the Oyashio region

In the top 200 m of the Oyashio region, dissolved Cd concentrations were much higher and $\delta^{114/110}$Cd were generally lighter than in the Kuroshio region, with Cd concentrations ranging from 0.39 nM to 1.1 nM and $\delta^{114/110}$Cd values ranging from +0.5 to +0.8‰ in the surface water then decreasing to +0.1 to +0.2‰ at 200 m. In the interval from 200 to 300 m, where OSMW is the major water mass, dissolved Cd concentration and the Cd isotopic value did not vary significantly (Fig. 3). At depths from 300 to 1000 m, dissolved Cd concentrations decreased by only 0.1 nM and the $\delta^{114/110}$Cd remained almost unchanged with depth. Below 2500 m, where the water is dominated by NPDW and CDW, dissolved Cd concentration and isotopic composition were highly constrained, with concentrations ranging from 0.80 to 0.91 nM and $\delta^{114/110}$Cd ranging from +0.1 to +0.3‰ over the 20 latitudinal degrees sampling range.

3.3. Spatial distribution of particulate Cd

Figs. 4 and 5 exhibit the horizontal and vertical distributions of particulate Cd elemental and isotopic composition in the top 200 m. Due to extremely low particle concentrations in the Kuroshio region, except station TR11, the particulate Cd mass collected in all of the other four stations of the Kuroshio region was insufficient to obtain reliable isotopic data (Table S4). Horizontally, comparable to dissolved Cd concentrations, the particulate concentrations show elevated concentrations in the Oyashio region and

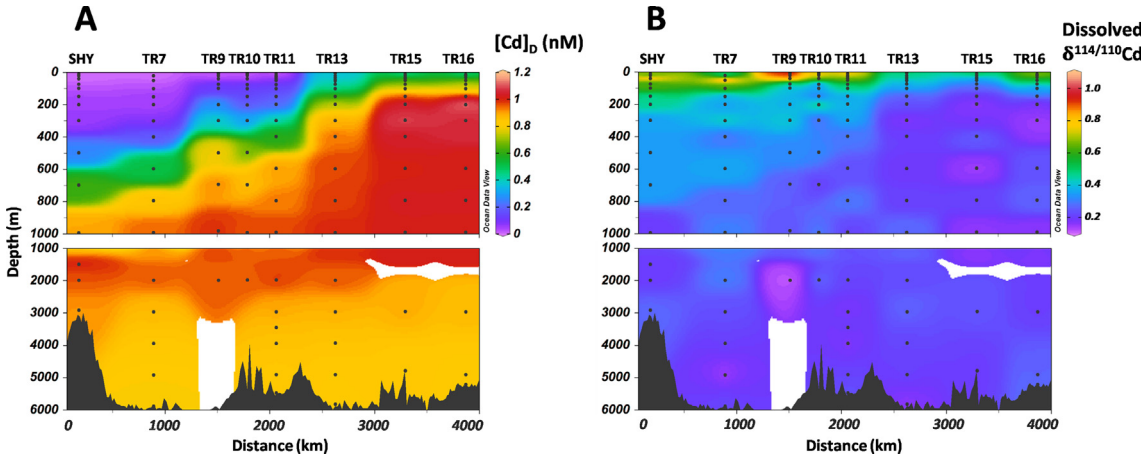

Fig. 3. Transects of dissolved Cd concentrations (A) and isotopic composition $\delta^{114/110}$Cd (B) of the studied region.

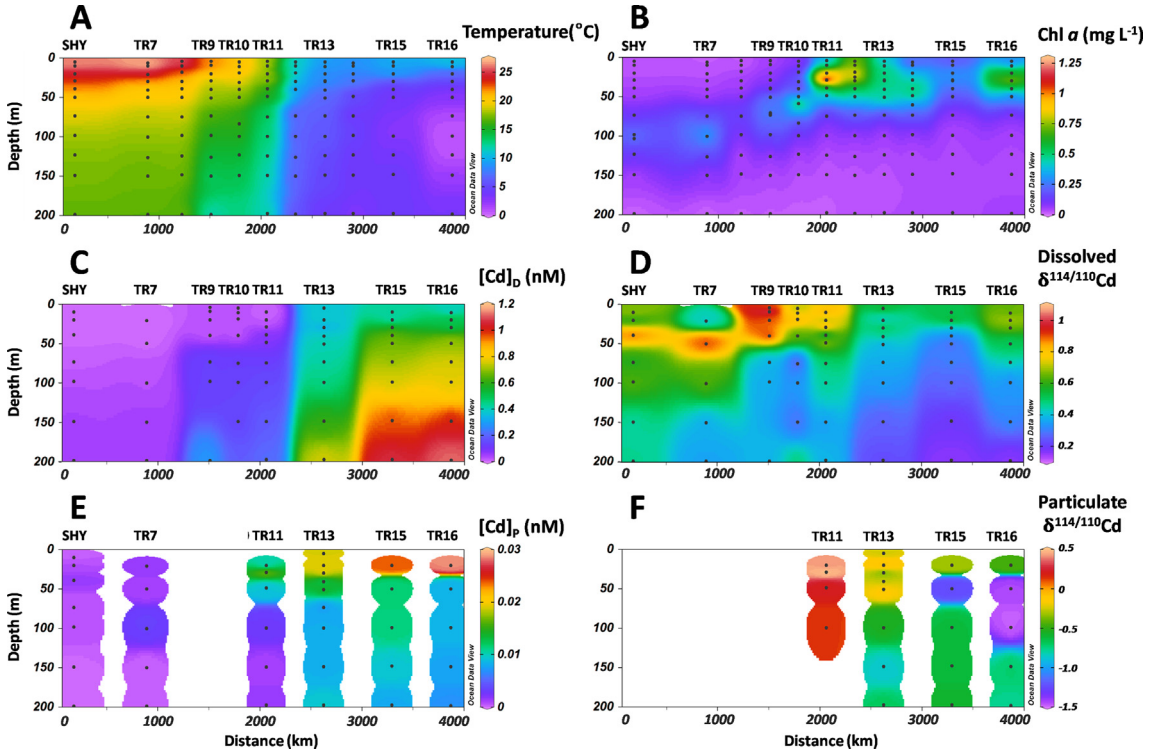

Fig. 4. Potential temperature (A), chlorophyll *a* concentration (B), dissolved Cd concentration and isotopic composition (C and D), and particulate Cd concentration and isotopic composition (E and F) transects in the top 200 m water layer of the studied region.

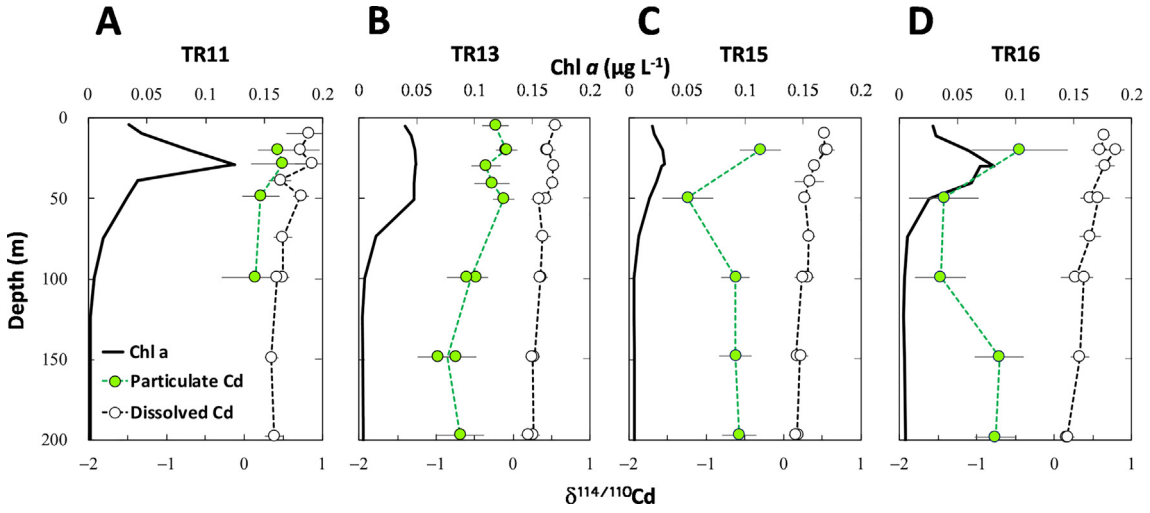

Fig. 5. Comparison of dissolved and particulate $\delta^{114/110}$Cd in the upper 200 m of TR11 (A), TR13 (B), TR15 (C), and TR16 (D). Green and open circles represent particulate and dissolved $\delta^{114/110}$Cd, respectively, and the black solid line represents chlorophyll *a* concentration.

extremely low concentrations in the Kuroshio region (Fig. 4E). Concentrations decreased down to 0.50 pM in the surface water of the southern stations of the Kuroshio region and increased up to 10 pM in the surface water of station TR11 (40°N). In the Oyashio region, particulate Cd concentrations ranged from 12 to 24 pM at TR 13 and 15 (45°N and 50°N) and reached 29 pM at TR16, which is the station in closest proximity to the Sea of Okhotsk. Vertically, particulate Cd concentrations show similar distribution patterns with chlorophyll *a* concentrations (Fig. 4B and E). However, the particulate Cd isotopic value varied drastically in comparison with dissolved Cd (Fig. 4F). The heaviest $\delta^{114/110}$Cd were observed at station TR11, a station in the Kuroshio region but closest to the extension interface, with values ranging from $+0.1 \pm 0.4$ to $+0.5 \pm 0.4$‰ (Fig. 5A). At station TR13, the most

southern station of the Oyashio region, the $\delta^{114/110}$Cd became lighter than at TR 11 and moderately decreased with depth. At station TR13 values were measured at -0.2 ± 0.1‰ in the upper 50 m, decreasing to -0.7 ± 0.2‰ in the zonation from 100 to 200 m (Fig. 5B). The most negative $\delta^{114/110}$Cd values were observed at the depths right below the chlorophyll *a* maximum depths of stations TR 15 and 16, the two most northern stations, with values ranging from -1.2 ± 0.3‰ to -1.5 ± 0.3‰ (Fig. 5C and D). Other than the lowest value, the particulate $\delta^{114/110}$Cd values ranged from -0.3 ± 0.3 to -0.8 ± 0.3‰, comparable to the values observed at station TR13 (Fig. 5B).

4. DISCUSSION

4.1. Cd cycling in the thermocline and deep water: the dominance of physical processes

In the thermocline and deep water, physical forcings are the dominant processes regulating Cd cycling, as shown by the comparable distribution patterns of elemental and isotopic composition of dissolved Cd to temperature (Figs. 2 and 3). The comparison of the Cd data with density has further validated the principal role physical processes play in regulating Cd cycling in the thermocline and deep water (Fig. 6A–C). In the deep water, where NPDW and CDW are dominant (Fig. 2A), concentrations range from 1.02 to 0.82 nM and σ_θ ranges from 27.5 to 27.8 (Fig. 6A). Here, the Cd concentration data obtained from different stations aligns perfectly on the same curve in a plot of dissolved concentrations versus σ_θ (Fig. 6A). In terms of dissolved $\delta^{114/110}$Cd in the deep water, the values are analytically indistinguishable, varying between $+0.12 \pm 0.11$ and $+0.30 \pm 0.10$‰ (Fig. 6B and C). These plots show that the end members of dissolved Cd concentrations are 1.02 and 0.82 nM for NPDW and CDW, respectively, but the Cd isotopic compositions are analytically indistinguishable between NPDW and CDW. For the zonation with σ_θ from 27.5 and 26.0 in the Kuroshio region, where upper NPDW, NPIW, and lower CMW are located (Fig. 2A), the datasets among different stations also systematically aligns on the same curve in a plot of dissolved concentrations versus potential density (Fig. 6A and B), indicating that physical processes including advection and mixing control the distribution of dissolved Cd concentrations and $\delta^{114/110}$Cd within this interval. Unlike the deep water zonation with analytically identical Cd isotopic values, $\delta^{114/110}$Cd slightly increases from $\sim+0.20 \pm 0.10$ to $\sim+0.41 \pm 0.10$‰ with decreasing depth or density within the range of 27.5–26.0 (Fig. 6B). Using σ_θ of 26.8 and 26.0 as representative densities for NPIW and lower CMW, respectively, the Cd concentrations and isotopic compositions of these water masses are around 0.70 nM and $+0.3 \pm 0.1$‰ and 0.19 nM and $+0.4 \pm 0.1$‰, respectively. NPIW, originating from the subarctic area, also reaches to the western Philippine Sea (WPS) and the South China Sea (SCS) (Qu et al., 2000). Our previous studies show that the concentrations decrease to ~0.64 nM in the WPS and further drop to ~0.60 nM in

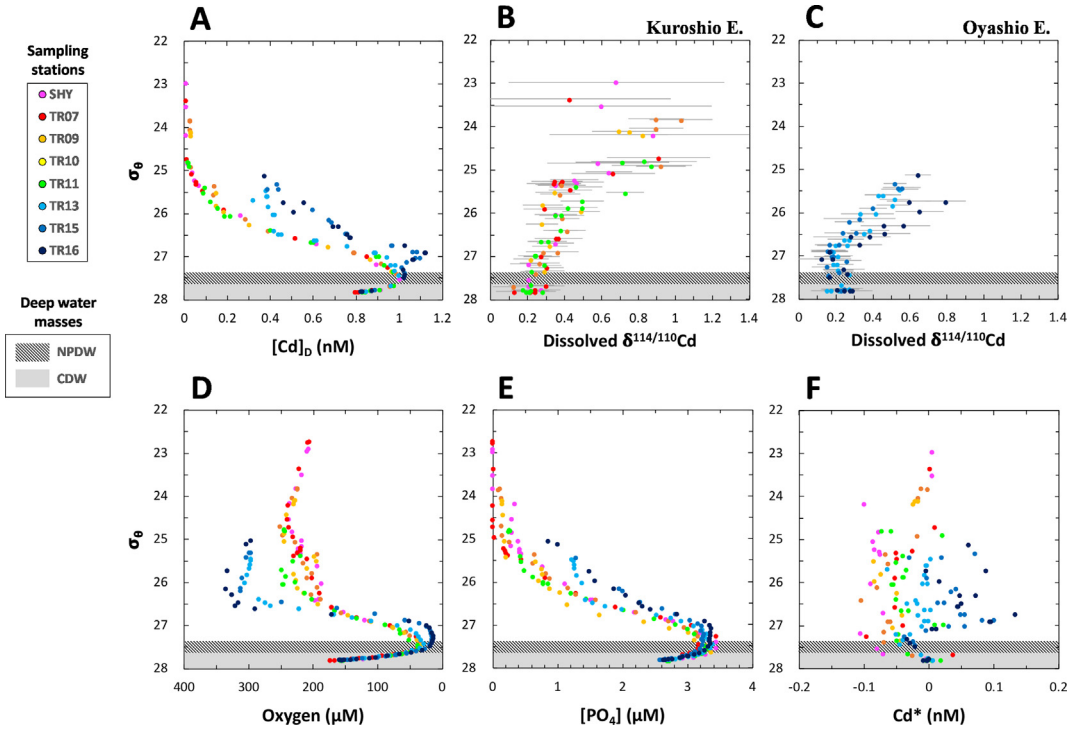

Fig. 6. Comparison of potential density (σ_θ) and dissolved Cd concentration (A), dissolved $\delta^{114/110}$Cd of the Kuroshio Extension region (B) and of the Oyashio Extension region (C), dissolved oxygen concentration (D), phosphate concentration (E), and Cd^* (F). Cd^* is calculated from the equation: $Cd^* = Cd_{measured} - (Cd/P_{deep} \times P_{measured})$. Here we use 0.32 mmol mol^{-1}, the averaged value of Cd/P ratios in NPDW and CDW in this study, as Cd/P_{deep} in the equation.

the northern SCS. Meanwhile the $\delta^{114/110}$Cd values elevate to around +0.4‰ in the WPS and SCS (Yang et al., 2012, 2015). The alteration of the Cd elemental and isotopic composition of NPIW among different longitudinal regions most likely reflects the effect of the progressive vertical mixing of NPIW with different upper water masses.

Table 1 compares the dissolved $\delta^{114/110}$Cd and dissolved Cd concentrations ($[Cd]_D$) in PDW and CDW observed in our and previous studies. This comparison shows that the Cd concentration and isotopic compositions in these same water masses are comparable to those in the North Pacific Ocean, indicating the Cd distribution over the deep water is governed by physical processes. Interestingly, we also found that $[Cd]_D$ in the water masses in the North Pacific are higher than the $[Cd]_D$ of the same water masses in the equatorial Pacific, whereas dissolved $\delta^{114/110}$Cd in the waters is consistent, ranging from +0.2 to +0.3‰. The elevated $[Cd]_D$ in the North Pacific indicates the deep waters accumulate Cd regenerated through deep water circulation pathways from the equatorial to the North Pacific Ocean. The comparable $\delta^{114/110}$Cd in the waters of these regions suggests the regenerated Cd possesses a similar isotopic composition as the deep water.

While the relationships with density in the thermocline and deep water exhibit consistent trends for almost all stations in this study, we observed extremely high dissolved Cd concentrations in the thermocline of stations TR15 and TR16 (Fig. 6A). In the interval of σ_θ from 27.5 to 26.7, equivalent to the interval of 1000–150 m (Fig. 2A), the dissolved Cd concentrations were up to 1.11 nM at a σ_θ of 26.9, even exceeding the concentrations observed in the deeper waters (Fig. 6A). The Cd isotopic composition was also slightly lighter in this interval than the value observed at the same density of other stations (Fig. 6B and C). These extremely high Cd concentrations suggest that there may be extra Cd source in this zonation. Vertically, the decomposition of sinking particles in the water interval may be a potential source for the abnormal Cd levels since particulate Cd concentrations in the euphotic zone of the two northern stations are relatively high (Fig. 4E). Previous studies have reported the concurrence of high Cd concentrations and low $\delta^{114/110}$Cd at the oxygen minimum and phosphate maximum zones in other oceanic regions and suggested that the abnormal Cd concentrations was attributed to the remineralization of organic matter (Xue et al., 2013; Abouchami et al., 2014). However, the σ_θ (26.9) with abnormally high Cd concentrations was lower (or shallower) than the σ_θ (27.2) of the oxygen minimum zone and the σ_θ (27.1) of the phosphate maximum zone (Fig. 6A, C, D and E). Previous studies also proposed that micronutrients may be remineralized more rapidly than macronutrients in organic matter and result in relatively shallow depths for their maximum concentrations (Janssen and Cullen, 2015; Janssen et al., 2017). In addition, the shelf sediments of the adjacent marginal seas may be a potential dissolved Cd source for the high Cd concentrations observed in TR15 and TR16. Indeed, previous studies found that the intermediate and deep waters of the Sea of Okhotsk possess relatively high dissolved Cd, ranging from 1.1 to 1.2 nM (Abe, 2002). Nishioka et al.

Table 1
Cd concentrations and isotopic compositions, and Cd/PO_4 ratios for major water masses in the intermediate and deep oceans in the N. Pacific.

Water mass	Region	Potential temperature (°C)	Salinity (psu)	$[O_2]$ (μM)	$[Si(OH)_4]_D$ (μM)	$[Cd]_D \pm 2SD$ (nM)	$Cd/PO_4 \pm 2SD$ (mmol mol^{-1})	$\delta^{114/110}Cd_D \pm 2SD$	n	Reference[a]
NPIW	N. Pacific	7.5–11.3	34.0–34.4			0.61 ± 0.38	0.32 ± 0.03	+0.40 ± 0.12	6	[1–4]
		4.3–7.8	34.0–34.1	81–171	49–88	0.70 ± 0.29	0.30 ± 0.03	+0.31 ± 0.09	11	This study
						0.67 ± 0.31	***0.31 ± 0.03***	***+0.34 ± 0.10***	***17***	***All NIPW data***
PDW	N. Pacific	1.3–2.0	34.6–34.7			0.94 ± 0.13	0.33 ± 0.03	+0.24 ± 0.10	19	[3–5]
		1.2–1.9	34.6–34.7	62–138	126–161	0.92 ± 0.08	0.31 ± 0.01	+0.22 ± 0.11	14	This study
						0.93 ± 0.11	***0.33 ± 0.03***	***+0.23 ± 0.10***	***33***	***All NPDW data***
	Eq. Pacific	1.2–2.0	34.6–34.7			0.77 ± 0.05	0.29 ± 0.04	+0.28 ± 0.16	250	[6]
CDW	N. Pacific	~1.2	34.7			0.86 ± 0.04	0.34 ± 0.06	+0.29 ± 0.12	4	[1,4]
		1.0–1.2	34.7	146–174	144–150	0.83 ± 0.03	0.32 ± 0.01	+0.21 ± 0.08	16	This study
						0.83 ± 0.03	***0.32 ± 0.03***	***+0.22 ± 0.09***	***20***	***All NCDW data***
	Eq. Pacific	0.9–1.2	34.7			0.72 ± 0.04	0.30 ± 0.01	+0.27 ± 0.08	11	[6]

The numbers with bold and italic format are the averaged value of the specified water masses of the North Pacific Ocean.
[a] [1] Ripperger et al. (2007); [2] Yang et al. (2012); [3] Yang et al. (2014); [4] Conway and John (2015); [5] Janssen et al. (2017); [6] John et al. (2017).

(2013) reported that high dissolved Fe originating from the sediments in the Sea of Okhotsk is transported into the intermediate water of the Northwest Pacific Ocean. Hydrographic data also showed that the contribution of Okhotsk Sea intermediate water to the Northwest Pacific is significant in the range from 26.7 to 27.4 (Yasuda et al., 2002), which is consistent to the σ_θ with the abnormally high Cd concentrations. Thus, the Okhotsk waters with high Cd concentrations are likely to be the major source of the elevated Cd concentrations observed in the thermocline of TR15 and 16. The spatial distribution of dissolved Cd and salinity in the thermocline of TR 15 and 16 also shows comparable patterns with the Sea of Okhotsk to the northwest Pacific (Fig. S2B and C). Using Cd^*, defined by the following equation, $Cd^* = Cd_{measured} - (Cd/P_{deep} \times P_{measured})$, as a tracer for Cd enrichment or depletion relative to phosphate, we have further confirmed that the water from the Sea of Okhotsk is a major Cd source of the excess Cd at around 200 m deep for TR15 and 16 by isopycnal mixing (Fig. S2D). Here we use a common Cd/P ratio, 0.32 mmol mol^{-1}, obtained by averaging Cd/P ratios in the deep water of the NPDW and CDW, to be Cd/P_{deep} as their ratios are statistically comparable (Table 1).

Cd sulfide formation is proposed to occur in the oxygen minimum zone (OMZ) of the subarctic northeast Pacific and tropical and subtropical Atlantic (Waeles et al., 2013; Janssen et al., 2014, 2017; Conway and John, 2015). This precipitation process is argued to be a significant sink of dissolved Cd in global oceans (Janssen et al., 2014). Our study region holds distinct OMZ with dissolved oxygen down to ~15 μM in the thermocline (Fig. 2C), which provides us with the opportunity to examine whether or not Cd sulfide precipitation is significant for dissolved Cd removal in the Northern Pacific Ocean. Contrary to the previous studies, we did not observe significant shifts in Cd/P ratios and Cd^* that would support the idea that Cd sulfide precipitation influences Cd isotopic compositions. The Cd/P ratios also did not show a systematic decrease in the OMZ (Fig. S3). The Cd^* values in the water columns ranged from +0.10 to −0.08 nM (Fig. 6F), indicating that Cd sulfide formation is insignificant in the studied site. Similarly, no significant Cd deficiency was observed in the OMZ of the eastern subtropical South Pacific (John et al., 2017). The argument of Cd sulfide precipitation in OMZ regions may therefore be incorrect.

4.2. Cd cycling in the surface water: open or closed system models?

Although biological activities are dominant processes determining Cd isotopic fractionation patterns in the euphotic zone, physical activities can still play a significant role in influencing the fractionation patterns in the surface water. Depending on the influential extent of physical forcing, two different models are proposed to explain Cd isotope fractionation patterns in the surface water as detailed in the introduction section. With intensively mixed surface water and elevated Cd input from the sub-surface water, the surface water of the Oyashio region should match a steady-state open system fractionation model. Contrarily, since the surface and subsurface waters in the Kuroshio region are highly stratified due to high water temperature and relatively weak wind strength during the summer season, the surface water of the Kuroshio region for Cd cycling is expected to agree with a closed system Rayleigh fractionation model. However, with similar correlation coefficients between the two model results and the measured value for stations TR 13, 15, and 16, the bio-

Table 2
Biological fractionation factors (α) estimated by open-system and closed-system models, as well as by suspended particles and dissolved Cd data in each of the sampling stations.

Sampling site	Open-system model[a]			Closed-system model[b]			$\delta^{114/110}Cd_P - \delta^{114/110}Cd_D$[c]	
	α	±2σ	r^2 [d]	α	±2σ	r^2 [d]	α	±2σ
TR7	1.0003	±0.0038	0.11	1.0001	±0.0002	0.43	n.a.[e]	n.a.
SHY	1.0003	±0.0020	0.18	1.0001	±0.0001	0.51	n.a.	n.a.
TR9	1.0006	±0.0006	0.62	1.0002	±0.0001	0.90	n.a.	n.a.
TR10	1.0004	±0.0007	0.39	1.0002	±0.0001	0.70	n.a.	n.a.
TR11	1.0004	±0.0005	0.58	1.0002	±0.0001	0.76	1.0003	±0.0003
TR13	1.0004	±0.0003	0.63	1.0003	±0.0001	0.75	1.0007	±0.0001
TR16	1.0009	±0.0003	0.77	1.0007	±0.0002	0.72	1.0010	±0.0006
TR15	1.0006	±0.0001	0.91	1.0004	±0.0001	0.96	1.0008	±0.0003

[a] The α values are obtained from dissolved Cd concentration and $\delta^{114/110}$Cd values by applying the open-system fractionation equation driven by Xie et al. (2017), $\delta^{114/110}Cd_{surface} = \delta^{114/110}Cd_{initial} + 10^3 \cdot (1 - 1/\alpha) \cdot (1 - [Cd]_{surface}/[Cd]_{initial})$, where $[Cd]_{initial} = 1$ nM and $\delta Cd_{initial} = +0.18$ for Oyashio Extension region and $[Cd]_{initial} = 0.35$ nM and $\delta Cd = +0.30$ for Kuroshio Extension region. The initial values are averaged $[Cd]_D$ and dissolved $\delta^{114/110}$Cd at 300 m of the extension regions.

[b] The α values are evaluated from dissolved Cd concentration and $\delta^{114/110}$Cd values using a Rayleigh fractionation equation (e.g. Ripperger et al., 2007), $\delta^{114/110}Cd_{surface} = \delta^{114/110}Cd_{initial} - 10^3 \cdot (1 - 1/\alpha) \cdot \ln([Cd]_{surface}/[Cd]_{initial})$, where the settings of $[Cd]_{initial}$ and $\delta^{114/110}Cd_{initial}$ are identical with that of the open-system model calculation.

[c] The α values are calculated from the isotopic difference between particulate and dissolved Cd at chlorophyll *a* maximum depth in each station.

[d] r^2 value represents the coefficient of determination for open-system or closed- system modeling of data for each station.

[e] n.a.: not available due to extremely low collected particulate concentrations.

logical fractionation effect may be reasonably explained by either the closed system or the open system model (Table 2). In the closed system model, the fractionation factors are 1.0003 ± 0.0001, 1.0004 ± 0.00011, and 1.0007 ± 0.0002 for TR13, 15, and 16, respectively (Fig. 7A). On the other hand, the fractionation can also be explained by the steady-state open system model, with α values to be 1.0004 ± 0.0003, 1.0006 ± 0.0001 and 1.0009 ± 0.0003, respectively, for stations TR13, 15 and 16 (Fig. 7B).

To directly estimate the fractionation factors, phytoplankton and biogenic suspended particles were collected at the same depths as the dissolved Cd samples in the top 200 m in this study (Fig. 5). Using the chlorophyll *a* maximum depth as an example, the particulate $\delta^{114/110}$Cd are -0.2 ± 0.1, -0.3 ± 0.3, and -0.5 ± 0.6‰ at these depths for stations TR13, 15, and 16, respectively (Fig. 5B–D). Corresponding dissolved $\delta^{114/110}$Cd values are $+0.5 \pm 0.1$, $+0.5 \pm 0.1$, and $+0.6 \pm 0.1$‰, respectively. First of all,

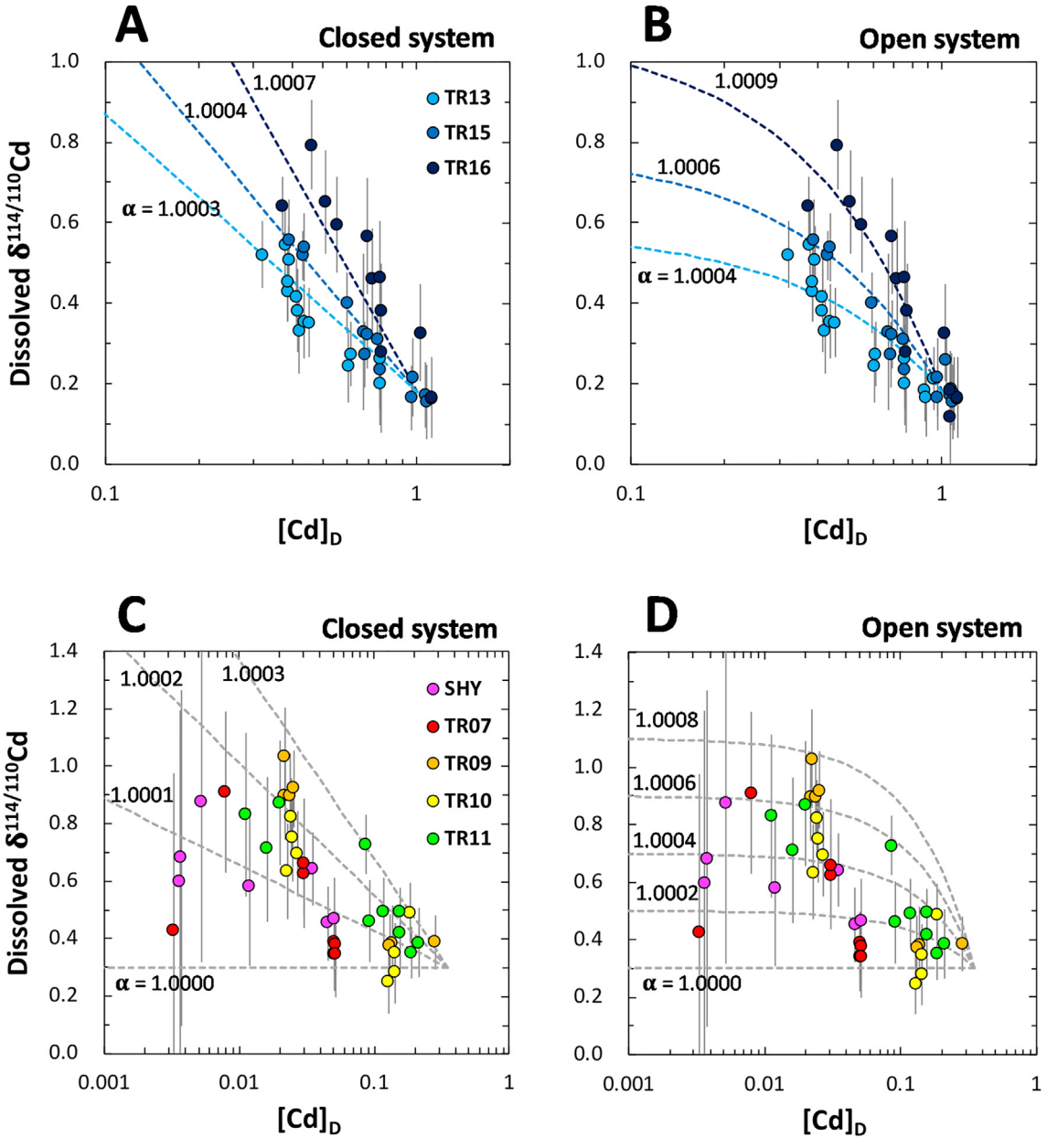

Fig. 7. Cd isotope systematics in the top 200 m water layer of the Oyashio Extension region (A and B) and Kuroshio Extension region (C and D). Closed system (A and C) and open system models (B and D) are applied to approximate the fractionation patterns. Model trend lines were calculated based on the initial conditions of $[Cd]_D = 1$ nM and $\delta^{114/110}Cd = +0.18$ for the Oyashio Extension region (A and B) and $[Cd]_D = 0.35$ nM and $\delta^{114/110}Cd = +0.30$ for the Kuroshio Extension region (C and D). The initial values are averaged $[Cd]_D$ and dissolved $\delta^{114/110}$Cd at 300 m of the extension regions.

the relatively low particulate Cd isotopic composition demonstrates that phytoplankton indeed assimilate isotopically light Cd and result in relatively heavy dissolved Cd in the surface water. Secondly, on the basis of the difference between dissolved and particulate Cd isotopic values at the same depths, the fractionation factors were 1.0007 ± 0.0001, 1.0008 ± 0.0003, and 1.0010 ± 0.0006 for TR13, 15, and 16 at the chlorophyll *a* maximum depths (Fig. 5), showing an increasing trend from the southern to the northern stations. These directly determined values are significantly closer to the values estimated from the open-system model than the closed system model for the Oyashio Extension stations (Fig. 8), supporting the scenario that the surface water of the Oyashio region matches the open system model (Fig. 5B). Here, we show the importance of particulate $\delta^{114/110}$Cd information for validating the Cd isotope fractionation process in oceanic surface water when dissolved $\delta^{114/110}$Cd alone is inadequate to assess this.

For the Kuroshio region, in terms of the closed system model, biological fractionation factors generally range from 1.0001 to 1.0002; in terms of the open system model, the factors range from 1.0003 to 1.0006 (Table 2; Fig. 7C and D). TR11 particulate samples were only available in the Kuroshio region (Fig. 5A) giving a fractionation factor of 1.0003 ± 0.0003 at the chlorophyll *a* maximum depth, which is in between the values estimated from the two models (Fig. 8). The value of the particulate data is hindered by the relatively large error bars of dissolved $\delta^{114/110}$Cd of the surface water samples in the Kuroshio region where the Cd concentrations were extremely low (Figs. 7 and 8). By comparing the linear correlation coefficients between modeled results and measured values, we thus examined the compatibility of the models to explain the Cd isotope fractionation patterns in the surface water. We found that the open system model yields significantly poorer linear correlation coefficients (r^2), ranging from 0.18 to 0.62, than the closed system model, which range from 0.43 to 0.90 (Table 2). The open system model also generates much larger uncertainties for α, ranging from ± 0.0006 to ± 0.0038, than the closed system model, which range from ± 0.0001 to ± 0.0002. Overall, the results from the open system model show a poor fit between the modeled dissolved $\delta^{114/110}$Cd results and measured values for most of the samples (Table 2). These results indicate that the closed system model matches the measured values in the surface water of the Kuroshio region. Just as the fractionation factors in the surface water of the Kuroshio region were much smaller than the value observed in the Oyashio region (Fig. 8), Cd fractionation factors appear to be highly spatially varied in the surface water of the ocean.

An anomalously light $\delta^{114/110}$Cd value, $+0.4 \pm 0.6‰$, was observed at 20 m at TR7, where the Cd concentration

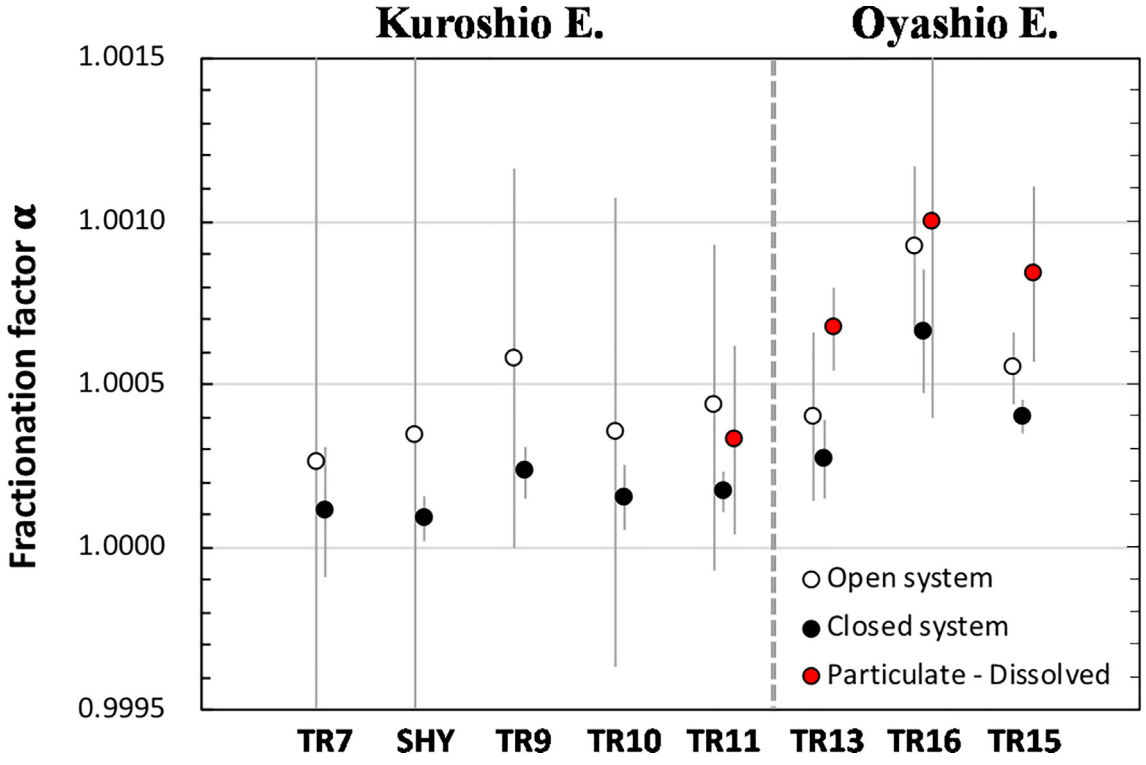

Fig. 8. Cd biological fractionation factor α in the surface water of the sampling stations. The data is arranged in order of the latitudes of the stations. Open circles represent α modeled by steady-state open system conditions; closed circles represent α modeled by closed Rayleigh fractionation system conditions; red circles represent actual measured values, which were obtained from the isotopic difference between particulate and dissolved Cd at chlorophyll *a* maximum depths. Dissolved Cd concentrations and isotopic data of the top 200 m in each water column were applied for model calculation. For the modeling of station TR7, an anomalously light $\varepsilon^{114/110}$Cd value in the very top of the surface water is excluded.

was only 3.3 pM. This Cd isotopic value significantly deviates from the modeled predictions of both the closed system and the open system models (Fig. 7C and D). Similarly, observations with abnormally light $\delta^{114/110}$Cd and extremely low Cd concentrations were reported in the surface or subsurface water of other oceanic regions (Ripperger et al., 2007; Gault-Ringold et al., 2012; Janssen et al., 2017; Xie et al., 2017). Analytical artifacts should not be excluded, in particular for oceanic surface waters possessing extremely low Cd concentrations, where some reported Cd isotopic values were extremely heavy. We thus support the initiative to carry out an inter-calibration exercise for the dissolved Cd isotopic measurement of oceanic surface waters where Cd concentrations are extremely low (Janssen et al., 2017; Xie et al., 2017).

The importance of horizontal mixing was also examined by comparing the linearity of $\delta^{114/110}$Cd–$[Cd]_D^{-1}$ with isopycnal lines in a two-end member mass balance mixing system (Fig. S4). If the data distribution pattern among different stations exhibit linear and parallel relationship with isopycnal lines in the figure, horizontal mixing may be significant at the depths of the stations. However, we found that there are only limited points following a linear relationship among the stations, mainly at σ_θ ranging from 26.4 to 26.2. Most of the data do not exhibit a linear relationship on the isopycnals, suggesting that horizontal mixing is not the dominant process determining the Cd isotope composition in the studied region. Since the direction of water flow is generally zonal in the Oyashio-Kuroshio extension studied region (Fig. 1A), it is thus expected that the horizontal mixing is insignificant through the meridional transect.

4.3. Factors controlling biological fractionation in the surface water

This study shows that the biologically controlled Cd isotope fractionation factors exhibited a dramatic shift from the Kuroshio to the Oyashio regions, with relatively low values ranging from 1.0001 to 1.0003 in the Kuroshio region and relatively elevated values ranging from 1.0005 to 1.0010 in the Oyashio region. The extension region thus provides us with an ideal opportunity to study the potential factors controlling Cd biological fractionation in the surface water. There are several environmental factors that may influence the isotope fractionation factors in the surface water, including temperature, trace metal interaction, phytoplankton community structure, and organic ligand complexation. Anomalously low temperatures were observed at the depths that also exhibited extremely negative particulate Cd isotopic compositions at 50 m of TR15 and 50 and 100 m of TR16, ranging from −1.2 to −1.5‰ (Fig. 4A and F). The low temperature water is attributed to the outflow of Subsurface Cold Water from the Sea of Okhotsk (Hill et al., 2003; Fig. S2). The coincidence of the low particulate $\delta^{114/110}$Cd and low temperature suggests that the particulate Cd might be associated with the outflow of the Sea of Okhotsk. In addition to the lateral transport of the water mass, water temperature has direct and indirect effects on biological Cd isotopic fractionation. We found that there were strong linear relationships between temperature and particulate $\delta^{114/110}$Cd or $\Delta^{114/110}$Cd, the fractionation effects between particulate and dissolved Cd (Fig. S5). It is also known that temperature is a critical factor determining phytoplankton community structure (Davison, 1991), which may influence Cd isotope fractionation factors. Laboratory phytoplankton culture studies are needed to evaluate the relative influence of temperature on the isotope fractionation processes.

Xie et al. (2017) proposed that the complexation of Cd with organic ligands may be an important process controlling the Cd isotopic composition in the surface water. They argued that this process could hamper the significant elevation in dissolved $\delta^{114/110}$Cd during phytoplankton Cd uptake. Although the argument may be a possible explanation for the Cd isotopic fractionation pattern observed in the surface water of Kuroshio extension region, there are no direct measurements of organic ligand Cd concentrations to support this argument. Further field studies and laboratory experiments of Cd isotopic fractionation for Cd speciation will help to evaluate the hypothesis.

Cd uptake in phytoplankton is known to be influenced by the availability of other dissolved trace metals in seawater, in particular Zn and Fe, or dissolved CO_2 (de Baar et al., 2017). Culture studies demonstrate that depleted concentrations of Zn and Fe in seawater strongly increase Cd uptake in some phytoplankton due to an up-regulation of divalent metal membrane transporters taking up Cd in addition to biodilution effects (Sunda and Huntsman, 2000; Lane et al., 2009). We found that trace metal availability varies significantly between the Oyashio and Kuroshio regions. The Oyashio surface water is known to originate from the Fe-limited High Nutrient Low Chlorophyll (HNLC) region (Nishioka and Obata, 2017), where Fe may be a limiting factor. Moreover, the ratio of dissolved metals to soluble reactive phosphorus concentrations is one to two orders of magnitude higher in the euphotic zone of the Kuroshio region than the Oyashio region (Fig. S6), illustrating the distinct trace metal conditions between the two regions. In addition, due to the enormous variations of chemical and physical conditions, phytoplankton community structures also show drastic changes between the extension regions, with chlorophytes, chrysophytes, and prymnesiophytes dominating in the Oyashio region (Suzuki et al., 2002) and cyanobacteria dominating in the Kuroshio region. Culture studies demonstrate that cyanobacteria are sensitive to Cd toxicity and possess relatively low Cd uptake rates (Brand et al., 1986; Payne and Price, 1999) and both chlorophytes and prymnesiophytes possess relatively high Cd cellular quotas or uptake rates, even one to two orders of magnitude higher than other major phyla (Sunda and Huntsman, 2000; Ho et al., 2003). Different phytoplankton groups may exhibit different affinities to trace metal transport and Cd uptake and result in different Cd isotopic discrimination. In addition to laboratory culture studies to investigate the relative influence of different phytoplankton groups on Cd isotope fractionation factors by varying trace metal availability, field shipboard incubation studies are essential to validate the findings of laboratory culture studies.

5. CONCLUSION

Our study demonstrates that biological fractionation effects vary dramatically in the surface water of the studied regions and many environmental factors can be responsible for the causes. However, the systematic variations of dissolved Cd and $\delta^{114/110}$Cd with density distribution patterns shows that physical mixing and advection are the principal forcings on Cd isotope fractionation patterns in the thermocline and deep water of the Oyashio and Kuroshio regions. We also observed that Cd sulfide precipitation is insignificant in the OMZ of our study region. In terms of the surface water, the Cd isotope fractionation systems closely correspond to the hydrographic features in the two contrasting extension regions, matching a steady-state open system fractionation model in the relatively well-mixed Oyashio Extension region and a closed system Rayleigh fractionation model in the highly stratified Kuroshio Extension surface water. Further laboratory culture and field incubation studies are required to decipher the relative contributions of biogeochemical and physical processes in controlling Cd isotopic cycling in the surface waters of the ocean.

ACKNOWLEDGEMENT

We thank the technical support of the personnel of R/V Hakuho-Maru, Chih-Ping Lee, Hsu-Han Yang, Wen-Hsuan Liao, Kuo-Fang Huang, and Der-Chuen Lee on sampling and analysis and Claudia Chern for proofreading this manuscript. We also thank Ruifang Xie, the other two reviewers, and associate editor Claudine Stirling for their helpful comments on this manuscript, which have significantly improved the quality of this paper. This research was financially supported by Taiwan Ministry of Science and Technology [grants numbers 104-2811-M-001-069 and 105-2119-M-001-039-MY3] and Career Development Award from Academia Sinica, Taipei, Taiwan.

APPENDIX A. SUPPLEMENTARY MATERIAL

Supplementary data associated with this article can be found, in the online version, at https://doi.org/10.1016/j.gca.2018.05.001.

REFERENCES

Abe K. (2002) Preformed Cd and PO_4 and the relationship between the two elements in the northwestern Pacific and the Okhotsk Sea. *Mar. Chem.* **79**(1), 27–36.

Abouchami W., Galer S. J. G., de Baar H. J. W., Alderkamp A. C., Middag R. and Laan P. (2011) Modulation of the Southern Ocean cadmium isotope signature by ocean circulation and primary productivity. *Earth Planet. Sci. Lett.* **305**, 83–91.

Abouchami W., Galer S. J. G., Horner T. J., Rehkämper M., Wombacher F., Xue Z., Lambelet M., Gault-Ringold M., Stirling C. H., Schönbächler M., Shiel A. E., Weis D. and Holdship P. F. (2012) A common reference material for cadmium isotope studies – NIST SRM 3108. *Geostand. Geoanal. Res.* **37**, 5–17.

Abouchami W., Galer S. J. G., de Baar H. J. W., Middag R., Vance D., Zhao Y., Klunder M., Mezger K., Feldmann H. and Andreae (2014) Biogeochemical cycling of cadmium isotopes in the Southern Ocean along the Zero Meridian. *Geochim. Cosmochim. Acta* **127**, 348–367.

Boyle E. A., Sclater F. and Edmond J. M. (1976) Marine geochemistry of cadmium. *Nature* **263**, 42–44.

Brand L. E., Sunda W. G. and Guillard R. R. (1986) Reduction of marine phytoplankton reproduction rates by copper and cadmium. *J. Exp. Mar. Bio. Ecol.* **96**(3), 225–250.

Cullen J. T. and Sherrell R. M. (1999) Techniques for determination of trace metals in small samples of size-fractionated particulate matter: phytoplankton metals off central California. *Mar. Chem.* **67**(3), 233–247.

Conway T. M., Rosenberg A. D., Adkins J. F. and John S. G. (2013) A new method for precise determination of iron, zinc and cadmium stable isotope ratios in seawater by double-spike mass spectrometry. *Anal. Chim. Acta* **793**, 44–52.

Conway T. M. and John S. G. (2015) Biogeochemical cycling of cadmium isotopes along a high-resolution section through the North Atlantic Ocean. *Geochim. Cosmochim. Acta* **148**, 269–283.

Davison I. R. (1991) Environmental effects on algal photosynthesis: Temperature. *J. Phycol.* **27**, 2–8.

de Baar H. J., van Heuven S. M., Abouchami W., Xue Z., Galer S. J., Rehkämper M., Middag R. and van Ooijen J. (2017) Interactions of dissolved CO2 with cadmium isotopes in the Southern Ocean. *Mar. Chem.* **195**, 105–121.

Fiedler P. C. and Talley L. D. (2006) Hydrography of the eastern tropical Pacific: a review. *Prog. Oceanogr.* **69**(2), 143–180.

Gault-Ringold M. and Stirling C. H. (2012) Anomalous isotopic shifts associated with organic resin residues during cadmium isotopic analysis by double spike MC-ICPMS. *J. Anal. At. Spectrom.* **27**, 449–459.

Gault-Ringold M., Adu T., Stirling C. H., Frew R. D. and Hunter K. A. (2012) Anomalous biogeochemical behavior of cadmium in subantarctic surface waters: mechanistic constraints from cadmium isotopes. *Earth Planet. Sci. Lett.* **341**, 94–103.

Hill K. L., Weaver A. J., Freeland H. J. and Bychkov, A. (2003) Evidence of change in the Sea of Okhotsk: implications for the North Pacific. Atmos.-Ocean 41(1), 49–63.

Ho T. Y., Quigg A., Finkel Z. V., Milligan A. J., Wyman K., Falkowski P. G. and Morel F. M. M. (2003) The elemental composition of some marine phytoplankton. *J. Phycol.* **39**, 1145–1159.

Ho T. Y., Chien C. T., Wang B. N. and Siriraks A. (2010) Determination of trace metals in seawater by an automated flow injection ion chromatograph pretreatment system with ICPMS. *Talanta* **82**, 1478–1484.

Janssen D. J., Conway T. M., John S. G., Christian J. R., Kramer D. I., Pedersen T. F. and Cullen J. T. (2014) Undocumented water column sink for cadmium in open ocean oxygen-deficient zones. *Proc. Natl. Acad. Sci.* **111**, 6888–6893.

Janssen D. J. and Cullen J. T. (2015) Decoupling of zinc and silicic acid in the subarctic northeast Pacific interior. *Mar. Chem.* **177**, 124–133.

Janssen D. J., Abouchami W., Galer S. J. G. and Cullen J. T. (2017) Fine-scale spatial and interannual cadmium isotope variability in the subarctic northeast Pacific. *Earth Planet. Sci. Lett.* **472**, 241–252.

John S. G. and Conway T. M. (2014) A role for scavenging in the marine biogeochemical cycling of zinc and zinc isotopes. *Earth Planet. Sci. Lett.* **394**, 159–167.

John S. G., Helgoe J. and Townsend E. (2017) Biogeochemical cycling of Zn and Cd and their stable isotopes in the Eastern Tropical South Pacific. Mar. Chem. 10.1016/j.marchem.2017.06.001.

Lacan F., Francois R., Ji Y. C. and Sherrell R. M. (2006) Cadmium isotopic composition in the ocean. *Geochim. Cosmochim. Acta* **70**, 5104–5118.

Lane E. S., Semeniuk D. M., Strzepek R. F., Cullen J. T. and Maldonado M. T. (2009) Effects of iron limitation on intracellular cadmium of cultured phytoplankton: implications for surface dissolved cadmium to phosphate ratios. *Mar. Chem.* **115**(3–4), 155–162.

Martin J. M. and Thomas A. J. (1994) The global insignificance of telluric input of dissolved trace metals (Cd, Cu, Ni and Zn) to ocean margins. *Mar. Chem.* **46**, 165–178.

Nishioka J., Nakatsuka T., Watanabe Y. W., Yasuda I., Kuma K., Ogawa H., Ebuchi N., Scherbinin A., Volkov Y. N., Shiraiwa T. and Wakatsuchi M. (2013) Intensive mixing along an island chain controls oceanic biogeochemical cycles. *Global Biogeochem. Cy.* **27**(3), 920–929.

Nishioka J. and Obata H. (2017) Dissolved iron distribution in the western and central subarctic Pacific: HNLC water formation and biogeochemical processes. *Oceanogr. Limnol.*, 10.1002/lno.10548.

Price N. M. and Morel F. M. M. (1990) Cadmium and cobalt substitution for zinc in a marine diatom. *Nature* **344**, 658–660.

Payne C. D. and Price N. M. (1999) Effects of cadmium toxicity on growth and elemental composition of marine phytoplankton. *J. Phycol.* **35**, 293–302.

Qu T. D., Mitsudera H. and Yamagata T. (2000) Intrusion of the North Pacific waters into the South China Sea. *J. Geophys. Res.* **105**, 6415–6424.

Ripperger S. and Rehkämper M. (2007) Precise determination of cadmium isotope fractionation in seawater by double spike MC-ICPMS. *Geochim. Cosmochim. Acta* **71**, 631–642.

Ripperger S., Rehkämper M., Porcelli D. and Halliday A. N. (2007) Cadmium isotope fractionation in seawater – a signature of biological activity. *Earth Planet. Sci. Lett.* **261**, 670–684.

Sohrin Y., Urushihara S., Nakatsuka S., Kono T., Higo E., Minami T., Norisuye K. and Umetani S. (2008) Multielemental determination of GEOTRACES key trace metals in seawater by ICPMS after preconcentration using an ethylenediaminetriacetic acid chelating resin. *Anal. Chem.* **80**, 6267–6273.

Sunda W. G. and Huntsman S. A. (2000) Effect of Zn, Mn, and Fe on Cd accumulation in phytoplankton: implications for oceanic Cd cycling. *Limnol. Oceanogr.* **45**(7), 1501–1516.

Suzuki K, Minami C., Liu H., and Saino T. (2002) Temporal and spatial patterns of chemotaxonomic algal pigments in the subarctic Pacific and the Bering Sea during the early summer of 1999. Deep Sea Res. Part II Topical Stud. Oceanogr. 49 24–25, 5685–5704.

Takano S., Tanimizu M., Hirata T., Shin K. C., Fukami Y., Suzuki K. and Sohrin Y. (2017) A simple and rapid method for isotopic analysis of nickel, copper, and zinc in seawater using chelating extraction and anion exchange. *Anal. Chim. Acta* **967**, 1–11.

Waeles M., Maguer J.-F., Baurand F. and Riso R. D. (2013) Off Congo waters (Angola Basin, Atlantic Ocean): a hot spot for cadmium-phosphate fractionation. *Limnol. Oceanogr.* **58**(4), 1481–1490.

Xie R. C., Galer S. J., Abouchami W., Rijkenberg M. J., de Baar H. J., De Jong J. and Andreae M. O. (2017) Non-Rayleigh control of upper-ocean Cd isotope fractionation in the western South Atlantic. *Earth Planet. Sci. Lett.* **471**, 94–103.

Xue Z., Rehkämper M., Horner T. J., Abouchami W., Middag R., van de Flierd T. and de Baar H. J. W. (2013) Cadmium isotope variations in the Southern Ocean. *Earth Planet. Sci. Lett.* **382**, 161–172.

Yang S. C., Lee D. C. and Ho T. Y. (2012) The isotopic composition of Cadmium in the water column of the South China Sea. *Geochim. Cosmochim. Acta* **98**, 66–77.

Yang S. C., Lee D. C., Ho T. Y., Wen L. S. and Yang H. H. (2014) The isotopic composition of cadmium in the water column of the West Philippine Sea. *Front. Mar. Sci.* **1**, 61.

Yang S. C., Lee D. C. and Ho T. Y. (2015) Cd isotopic composition in the suspended and sinking particles of the surface water of the South China Sea: The effects of biotic activities. *Earth Planet. Sci. Lett.* **428**, 63–72.

Yasuda I., Kouketsu S., Katsumata K., Ohiwa M., Kawasaki Y., Kusaka A. (2002) Influence of Okhotsk Sea intermediate water on the Oyashio and North Pacific intermediate water. J. Geophys. Res. Oceans 107(C12), 30-1–30-11.

Yasuda I. (2003) Hydrographic structure and variability in the Kuroshio-Oyashio transition area. *J. Oceanogr.* **59**(4), 389–402.

Yasuda I. (2004) North Pacific intermediate water: progress in SAGE (SubArctic Gyre experiment) and related projects. *J. Oceanogr.* **60**(2), 385–395.

You Y., Suginohara N., Fukasawa M., Yasuda I., Kaneko I., Yoritaka H. and Kawamiya M. (2000) Roles of the Okhotsk Sea and Gulf of Alaska in forming the North Pacific intermediate water. J. Geophys. Res. Oceans 105(C2), 32-53–32-80.

Associate editor: Claudine Stirling